

# Optical Performance Monitoring for Intelligent Networks

Trevor Anderson<sup>(1,2)</sup>, Jonathan C. Li<sup>(1)</sup>, Don Hewitt<sup>(1)</sup>, Olivier Jerphagnon<sup>(1)</sup>

<sup>(1)</sup> Monitoring Division Inc, Melbourne, VIC 3002 Australia, [trevor@monitoringdivision.com](mailto:trevor@monitoringdivision.com)

<sup>(2)</sup> National ICT Australia Ltd (NICTA), Victoria Research Laboratory

**Abstract** *Optical Performance Monitoring is a key enabler for fully reconfigurable and transparent optical networks. In this paper we review the technologies and challenges for monitoring 40G/100G networks with an emphasis on multi-impairment monitoring solutions*

## Introduction

The introduction of high capacity reconfigurable optical networks offers the potential for lowering network costs and simplifying operations through automated path provisioning, fault management and network optimisation [1,2]. Importantly, these networks provide a means of handling rapidly expanding and unpredictable traffic demands across a variety of services. However, realizing this potential requires a real time picture of the optical impairments inside the network and their distribution.

Automated path provisioning, either for new services or load balancing presents challenges as time varying physical impairments may limit the feasibility of potential light paths. For 40 G signals, link penalties will include the impact of simultaneous impairments such as OSNR, chromatic dispersion, PMD, non linear effects and both inter-channel and interferometric crosstalk. Accurate monitoring of these parameters will improve utilisation through reduced system margins.

Self diagnosis and localisation of faults on transparent networks will require distributed monitoring; end to end signal quality measures will not provide the information. Similarly networks carrying alien wavelength will require physical layer monitoring for service quality assurance. Finally monitoring is required for feedback to tuneable compensation elements for automated network optimisation.

We envision that ubiquitous optical performance monitors are distributed throughout the network. The monitors should be capable of measuring multiple simultaneous impairments on multiple bit rates and

formats on a millisecond timescale. Our proposed solution consists of a low cost common sensor based on asynchronous delay tap technique [3]. The sensor has access to a library of pattern recognition algorithms for new formats and impairments. The key point is that the hardware platform is future proof, new formats or impairments are enabled with software upgrades. In this paper we describe recent multi-impairment monitoring work focussing on the asynchronous delay tap technique. To begin with however, we briefly review recent work on end to end monitoring with coherent receivers.

## Multi Impairment Monitoring

### End to End Monitoring with Coherent Receivers

It has recently been shown that the information available from equalisation filters of coherent receivers can be used to determine CD, PMD and PDL [4]. In this approach, the frequency dependence Jones Matrix,  $H(\omega) = A(\omega)U(\omega)D(\omega)$ , extracted from the filter is decomposed in to three factors where the PMD element is described by a unitary matrix  $U(\omega)$ , the PDL element by  $A(\omega)$ , and a scalar function  $D(\omega)$  contains information on amplitude filtering and CD. This technique was demonstrated on a 43 Gbit/s polarization multiplexed QPSK system and obtained a DGD accuracy of 7 ps and CD accuracy of 90 ps/nm over ranges of 0 to 90 ps and +/- 4000 ps/nm respectively. In a similar manner it has also been recently shown that CD, OSNR and Q can be measured with a coherent OFDM receiver [5]. We note that although these results are impressive, and come at no additional hardware cost at the receiver, the real time sampling requirements make them practical only for end to end monitoring. For distributed applications such as monitoring at a ROADM site for automated path selection a lower cost solution is needed.

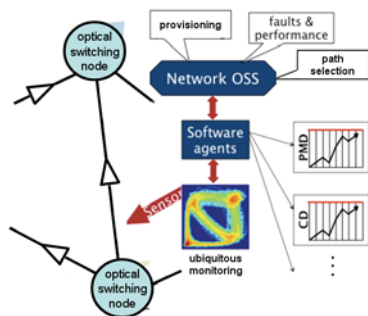


**Fig. 1:** Intelligent network with software algorithms enabling real time monitoring of multiple format and impairments from signals captured with a common sensor.

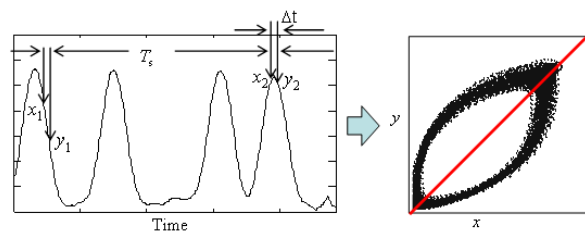


**Fig. 2:** Generation of phase portrait for 10Gbit/s NRZ with 1/4 bit delay.

*Distributed monitoring: Asynchronous delay-tap sampling*

Asynchronous delay-tap sampling is an alternative to the eye diagram [6] that uses the joint probability density function (pdf) of a signal  $x(t)$ , and its delayed version  $x(t+\Delta t)$  to characterize the signal [3,7]. To generate the phase portrait, the waveform is sampled in pairs separated by a known delay  $\Delta t$ , as shown for the NRZ signal in Fig. 2. The phase portraits contain unique impairment signatures that can be discovered using statistical pattern recognition techniques. With this approach we are able to not just classify impairments, but to quantitatively monitor simultaneous combinations. Results for 10 Gbit/s NRZ have shown the potential for simultaneous monitoring of OSNR, CD, DGD, crosstalk and optical filter detuning, Self phase modulation, as well the ability to measure signal quality parameters Q and timing jitter [7].

A key advantage of the technique is that a simple direct detection receiver can be used to monitor both amplitude and phase modulated formats without the need for demodulation of the signal or modification of the receiver bandwidth. For phase modulated formats we find that the intensity variations intrinsic in the format, together with the phase to amplitude conversion provided by the channel filter, is sufficient to monitor impairments.

*Analysis of Phase portraits*

Phase portraits can be treated as images and lend themselves well to a variety of image recognition techniques [8-10] we briefly describe two alternative approaches before introducing our own.

The  $\frac{1}{4}$  bit phase portrait as shown in Fig. 2 provides a convenient monitor of signal quality. The width of the minor axis is a measure of the slope of the waveform whilst the distribution along the major axis, (corresponding to zero slope) provides an approximate measure of the Q factor. In the approach adopted by [11] this Q estimate is used to monitor OSNR and the width is used to monitor CD. (In practice the width is obtained by using an image

processing technique known as a Hopf transformation). The technique was demonstrated for a 10 Gbit/s RZ DPSK signal for OSNR and CD. A key problem with this procedure however, is the cross coupling of OSNR and CD which limits the sensitivity and the ability to separate impairments.

An alternative model that overcomes the coupling between impairments [12] uses artificial neural networks to map phase portrait features onto the three impairments - OSNR, CD and DGD. The features used to describe the phase portrait denoted by  $(\bar{r}_1, \sigma_1, \bar{r}_3, \sigma_3, \bar{x}_2, \bar{y}_2, Q_{31})$  are obtained by dividing the portrait into quadrants as shown in Fig. 3a. Here  $\bar{r}$  and  $\sigma$  represent the expected value and standard deviation of the radial coordinate in the first and third quadrants respectively with  $\bar{x}_2$  and  $\bar{y}_2$  representing the mean values of the first and second samples in the 2<sup>nd</sup> quadrant. The 4<sup>th</sup> quadrant was not used as it was assumed to be symmetric with respect to the 2<sup>nd</sup>. The final parameter is similar to the approximate Q factor described above; it is defined as  $Q_{31} = (\bar{r}_3 - \bar{r}_1)/(\sigma_1 + \sigma_3)$ . Using this approach a correlation coefficient between input and output predictions of 0.97 was obtained for a simulated 10 Gbit/s NRZ system with relatively few (140) training cases. An important limitation of this result however was the restriction to worst case DGD with equal power splits in the principle states. (For a general PMD power split ratio,  $\gamma$ , the phase portrait is not symmetrical about the  $y = x$  axis).

Whilst the features used in the above approaches have the advantages of being interpretable, they are applicable for only a restricted range of formats and impairments. For this reason, the approach used by the authors is to automate the feature selection. The first step in the training process is to bin the sample pairs into a two dimensional histogram. For the work presented here a 30 by 30 histogram was used and all 900 features (representing the number of hits in each bin) are available for training. A key advantage of this approach is that it can be used for any format or tap delay without the need for fine tuning of the algorithm.

In our approach we use kernel based regression techniques to model the impairments. The predictors for each of the impairments can, in general, be assumed to be a weighted sum of the non-linear products of the feature vector to be measured and the phase portraits in the training set. The training process determines the weights which jointly minimises the sum of the squared errors and a regularisation term, the latter of which is used to avoid over fitting [9,10]. Once the data set sets are collected (this is the time consuming component) the optimised features and weights are determined within 30 s. In practice, the training sets are created using a "network emulator" to add known quantities of the

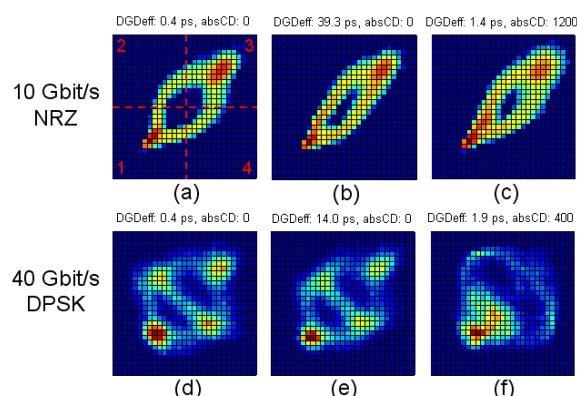


**Fig. 3:** Experimental phase portraits showing effects of CD and DGD, the OSNR is 14 dB for all cases. The tap delay was set at 25 ps in both cases.

impairments to a clean signal.

**Impairment Emulator and Monitor**

A schematic of the set up used to generate the training sets is shown in Fig. 4. The Impairment Emulator adds known combinations of DGD, CD and OSNR. A polarisation controller was used at the input to the DGD emulator to ensure a random alignment of polarisation states. CD was controlled using a tuneable dispersion compensation module. The OSNR is generated by coupling in filtered and amplified ASE noise.

In the monitor, the signal is filtered using a 30 GHz tuneable optical filter then fed to a 20 GHz receiver followed by a 50:50 splitter with a tuneable electrical delay set to 25 ps in one arm. The signal and delayed ports are sampled at 100 ks/s. 40k sample pairs are collected for each phase portrait.

We note that the 30 GHz (@3dB) tuneable optical filter used in our technique serves to both select the channel and to provide amplitude to phase conversion for 40G/100G formats. (In an alternative approach [13] a homodyne receiver is used to extract separate phase portraits for the phase and amplitude component of the signal).

**Results and Discussion**

In our first experimental demonstration of the technique [3] the impairments included were OSNR, CD and DGD where the latter was restricted to worst case polarization alignment of the signal and the principal states. More recently we have demonstrated the technique at 10 Gbit/s taking into account both the differential group delay (DGD) and a random power split between principal states. To do this we define an effective differential group delay  $DGD_{eff}$  [14] that is related to first-order string length and is a measure of first-order PMD system penalty [15]. When the signal is aligned with either principal state of polarization (PSP) ( $\gamma = 0$  or  $1$ )  $DGD_{eff} = 0$  and the signal remains undistorted regardless of the level of first-order PMD. The advantages of using  $DGD_{eff}$  are that it is directly related to the induced signal distortion and thus the 1st order PMD-induced system penalty, and it provides a dynamic measure for feedback for PMD compensation.

The results for a 10 Gbit/s NRZ and 40 Gbit/s DPSK signal are shown in Fig. 5 with typical phase portraits shown in Fig. 3. Although not shown here, a

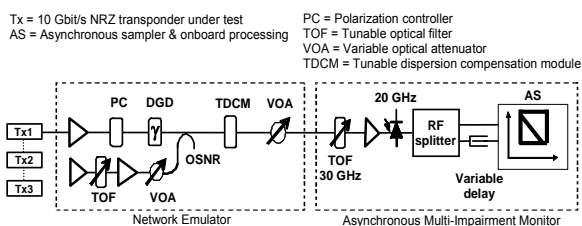


**Fig. 4:** Setup for generation of training sets. The impairment emulator adds known combinations of CD, 1st order PMD and OSNR to transponder signals.

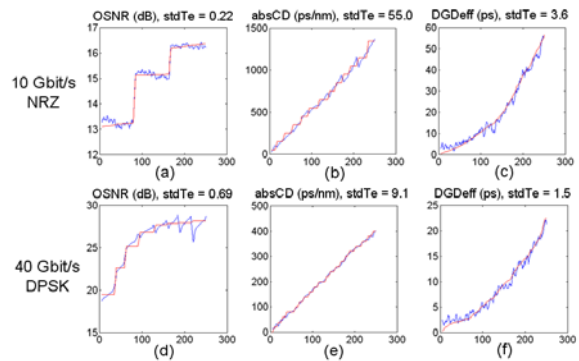


**Fig. 5:** Experimental measurements (blue) of simultaneous impairments for 10 Gbit/s NRZ and 40 Gbit/s NRZ DPSK. Results for 250 test cases are ordered along x axis by true values (shown in red). The test errors  $stdTe$  are quoted for the  $2\sigma$  level.

breakdown of the accuracy of the  $DGD_{eff}$  results for 10 G NRZ shows an expected degradation for poor OSNR and high CD values [14]. In contrast for DQPSK, the  $DGD_{eff}$  accuracy degrades with poor OSNR but surprisingly improves with increasing CD. A possible interpretation of this is that the CD induced phase to amplitude conversion provides a larger waveform for  $DGD_{eff}$  to distort.

The previous results can only be regarded as proof of principle since they have used training and test sets generated from the same transponder and impairment emulator. Tests for transponder dependency were performed on three commercial 10G transponders. The results for different combinations of training sets are shown in Table 1. We find that training and testing on separate transponders can give rise to significant errors. Training sets from combined transponders however add robustness to the measurements. Verification of the impairment emulator is shown in test results on independent impairments in Table 2.

In this case the CD for test cases is generated from varying lengths of SMF fibre and the PMD from birefringent fibre. For further verification, the technique has been recently demonstrated used on an 800 km 10G WDM test bed that includes ROADMs [16]. Measurements of CD and OSNR at multiple tap points were shown to have an accuracy of 30ps/nm and 0.5 dB respectively.

In work to date, it has been assumed that monitor has access to knowledge of the formats and bit rates being monitored from the network management system and can select appropriate predictors from an on board library. For the

**Table 1:** Test errors for Tx2 using different combinations of transponders in training.

Training set	OSNR (dB)	absCD (ps/nm)	DGD <sub>eff</sub> (ps)
Tx3	0.6	51	2.8
Tx1Tx3	0.7	45	2.6
Tx1Tx2Tx3	0.5	40	2.5
Tx2	0.4	26	2.1

**Table 2:** Independent validation of Impairment emulator

	OSNR (dB)	absCD (ps/nm)	DGDeff (ps)
true	13.0	0	9.0
measured	13.3	-55	9.3
true	13.0	0	14.0
measured	13.4	-8	15.2
true	13.0	576	0.0
measured	13.7	572	1.6
true	13.0	576	9.0
measured	13.2	547	7.1
true	13.0	576	14.0
measured	13.2	557	13.0

monitoring of systems with alien wavelengths, this information may not be available and automatic identification of format would be required. Automatic format and bit rate identification is a feature that the technique is well suited to. As an example, we have demonstrated that a single predictor can predict impairments at both 10.0 and 10.7 Gbit/s FEC rates. In principle, in order to make the technique more robust, one can extend the training set to include other effects which can potentially induce errors; these may include optical nonlinearities, filter drift and delay variations.

For the experimental setup described in this paper the measurement time was 1.2 s. This is dominated by the sampling time; the processing time required for prediction taking less than 20 ms. In future implementations, cost effective solutions at sampling rates of 50 MS/s will be achievable with currently available sample and hold technology. This will enable measurement times of better than 50 ms and provide an increased ability to exploit the improvement in accuracy that is achievable through averaging of multiple measurements.

*Application to higher order formats*

A key advantage of our approach is that it can be applied without the need for fine tuning of features or modification of hardware. For example, using the same algorithms and hardware as used for 10G NRZ and 40 G NRZ DPSK, we find that simulations of 40 Gbit/s RZ-DQPSK (see Fig. 6) and 100 Gbit/s 8 PSK give results, that are consistent with accuracies for simultaneous CD and DGD<sub>eff</sub> presented in this paper. In addition, the ability of the machine learning techniques to discern patterns in very “unstructured”

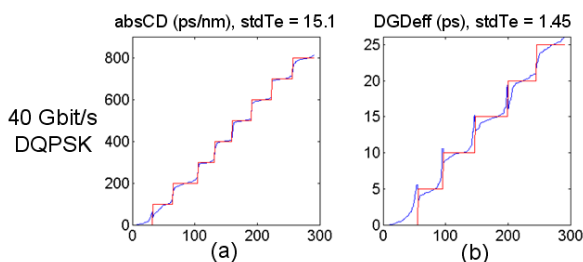


**Fig. 6:** Simulation results for simultaneous measurements of abs CD and DGD<sub>eff</sub> for 40 Gbit/s RZ -DQPSK. The OSNR ranged from 14 to 28 dB.

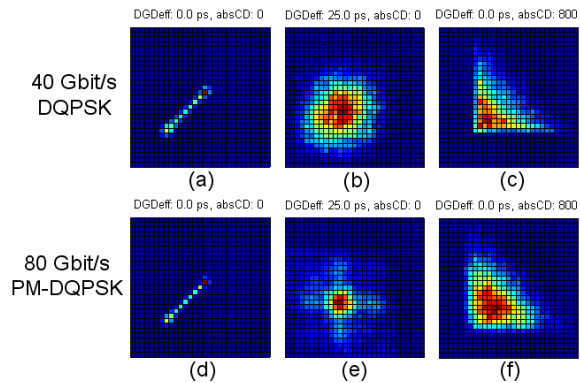


**Fig. 7:** Simulated phase portraits showing effects of 25ps of DGD (b), (e) and 800 ps/nm CD (c), (f) for 40 G RZ-DQPSK and 80 G PM-DQPSK signals

phase portraits holds promise for application of the technique to the monitoring of polarization multiplexed systems. By way of example, in Fig. 7, we show simulated phase portraits for 40 Gbit/s RZ-DQPSK and 80 Gbit/s Polarization multiplexed QPSK signals for a range of impairment levels. We emphasize that these results have been obtained with same direct detection based monitor used for 10G NRZ signals.

**Summary**

Embedded into next generation systems, in-line optical performance monitoring will open the door to improved system performance with active compensation using feed back control, and to optimised network provisioning. Networks will be able to locate where faults occur and recover from them. In this paper we show that the asynchronous delay tap sampling technique is a promising monitoring solution that uses a simple direct detection receiver, that combined with pattern recognition techniques, is capable of monitoring multiple formats and impairments. Finally, our results suggests that the ability of the machine learning techniques to discern patterns in very “unstructured” phase portraits holds promise for application of the technique to the monitoring of polarization multiplexed systems and the “next generation” of critical impairments.

**References**

1. A. Willner et al, *Optical Fiber Telecommunications*. V11B. Academic 2008.
2. D. Kilper, JLT, 22, pp 294-304, 2003.
3. T. Anderson et al., ECOC 2007.
4. J. C. Geyer et al. PTL 20(10), pp. 776-778, 2008.
5. W. Sheih et al. Optics Exp. 15(2), pp. 350, 2007.
6. R. A. Skoog et al., PTL 18(20), pp. 2398, 2006.
7. S. D. Dods et al., OFC/NFOEC, 2006, ThP5.
8. J. Zhao et al. CLEO/QELS 2008.
9. V. Vapnik, *Statistical Learning Theory*. Wiley, 1998.
10. R. Duda et al., *Pattern Classification*. Wiley, 2000.
11. B. Kozicki et al., Optics Exp., 16, pp.3566, 2008.
12. J. Jargon et al., OFC 2009, OTH11th.
13. H. Choi et al., OFC 2009 , ThJ5.
14. T. Anderson et al., OFC 2009, ThH7.
15. K. E. Cornick et al., PTL, 18, pp. 1149-1151, 2006.
16. T. Anderson et al., ECOC 2009.